# Soybean oil methanolysis over scallop shell-derived CaO prepared via methanol-assisted dry nano-grinding

# Soybean oil methanolysis over scallop shell-derived CaO prepared via methanol-assisted dry nano-grinding

Frisda R. Panjaitan[a], Shinya Yamanaka[b,]*, Yoshikazu Kuga[b]

[a]Division of Engineering, Muroran Institute of Technology, Mizumoto-cho 27-1, Muroran 050-8585, Japan
[b]College of Environmental Technology, Muroran Institute of Technology, Mizumoto-cho 27-1, Muroran 050-8585, Japan
Corresponding author. Tel.: +81 143 46 5747; fax: +81 143 46 5701
E-mail address: syama@mmm.muroran-it.ac.jp (S. Yamanaka)

## A B S T R A C T

Calcium oxides with a specific surface area between 4.5 $m^2g^{-1}$ and 62.5 $m^2g^{-1}$ were obtained by calcination of scallop shells, following by methanol-assisted dry nano-grinding. Three distinct phases are formed on the surface of these catalysts during nano-grinding: calcium methoxide, calcium hydroxide, and calcium oxide. The effects of specific surface area and active surface phase composition on the catalytic activity of calcium oxide during methanolysis of soybean oil were investigated. The properties of the calcium oxide before, during, and after methanol assisted dry nano-grinding were studied by XRD, FTIR, and nitrogen gas adsorption based on the BET method. The ground calcium oxides were found to be effective in catalyzing the methanolysis of soybean oil, with the optimal catalyst producing a 72.3% ester yield after 20 mins of reaction. The improvements in rate of reaction were attributed to the rapid formation of calcium diglyceroxide during the initial stages of methanolysis. A combination high specific surface area and effective active phases on the surface of the calcium oxide catalysts is correlated with reductions in mass transfer limitations in the early steps of the reaction, indicated by the rapid formation of calcium diglyceroxide.

Keywords: scallop shell, nano-grinding, methanolysis, specific surface area, active phases.

## 1. Introduction

Calcium oxide (CaO) is the most widely used and well-researched catalyst material for the heterogeneous methanolysis of oils to biodiesel. The suitability of

CaO to this application arises from its high basicity, low solubility in organic solvents, and its effectiveness under mild reaction conditions. Moreover, CaO feedstocks are plentiful with sources including natural carbonate-rich minerals such as dolomite, calcite, limestone, and shells from marine life [1, 2]. Since the reaction occurs on the surface of the catalyst, the major factors governing the performance of CaO are: the specific surface area, SSA, which largely determines the number of molecules which are able to adsorb to the material; high basicity of the active sites of reaction (or active phases on the surface of the catalyst); and catalyst particle size [2–8]. Many investigations have confirmed that CaO catalysts with a high SSA, strong basicity of surface reaction sites, and lower particle size accelerate the conversion rate, particularly in terms of facilitating the access of reactant molecules to basic sites on the catalyst surface. Reddy *et al.* [4] synthesized nano-sized CaO (nano-CaO) from *Polymedosa erosa* with a diameter and SSA of 66 ± 3 nm and 90.61 $m^2g^{-1}$, respectively, using a calcination–hydration–dehydration technique, and reported a 98.54% biodiesel yield. Kouzu *et al.* [9] derived CaO from natural limestone (SSA = 13 $m^2g^{-1}$) by calcination of pulverized limestone at 900 °C in a He gas flow, obtaining a 93% biodiesel yield. Wilson *et al.* [10] derived CaO from natural dolomitic rock by calcination at 900 °C, yielding particulates with SSA = 8 $m^2g^{-1}$, and reporting a 100% conversion of triglyceride in a transesterification reaction after 3 h. Buasri *et al.* [11] utilized CaO synthesized from mussel shells (SSA = 89.91 $m^2g^{-1}$), cockle shells (SSA= 59.87 $m^2g^{-1}$), and scallop shells (SSA= 74.96 $m^2g^{-1}$) for biodiesel production from palm oil. Lastly, Moriyasu *et al.* [12] reported a SSA of 13.6 $m^2g^{-1}$ and particle diameter 0.5 μm for CaO particles synthesized from calcined limestone by wet mechanical grinding.

Furthermore, the presence of active phases on the surface of the CaO catalyst has also been identified as an influence on the catalytic process: methanolysis reactions proceed via surface $OH^-$ groups which have been found to be present at basic sites on the catalyst surface [13, 14]. Thus, the catalytic behavior in the transesterification reaction is also determined as a function of the adsorbate coverage of the catalyst surface [8]. Kouzu *et al.* [15] and Refaat [16] have stated that the order of reactivity for active phases is $CaCO_3 < Ca(OH)_2 < CaO < Ca(OCH_3)_2$. Mass transfer resistance is a strong factor in determining the overall rate of the heterogeneous methanolysis reaction due to the immiscibility between the nonpolar triglyceride phase and the polar methanol phase. Ivana *et al.* [17] reported that calcium diglyceroxide (CaDg) acts as an emulsifier and suppresses the mass transfer resistance by increasing the interfacial area between methanol and oil: in this study, the CaO catalyst was transformed into CaDg by interaction with glycerol during the early stages of the methanolysis reaction [18].

Nano-grinding is a simple comminution process, which can produce ultra-fine particles (< 10 μm) with high SSA [19, 20]. The nano-grinding process can alter the size, structure, composition, and morphological characteristics of materials by carefully choosing the appropriate parameters [21, 22]. To date, little research has been reported on the use of mechanical activation to improve the catalytic properties of solid CaO with a view to biodiesel production [17, 23]. As such, in this study, a methanol assisted, dry nano-grinding process was employed to enhance the catalytic properties of CaO derived from scallop shell (CaO-ss). We report a comparison between two methods of nano-grinding, batchwise and stepwise addition of methanol, which produce catalytic powders with differing SSAs and differing degrees of active phases on the material surface.

Reducing mass transfer limitation during the initial stages of the heterogeneous methanolysis reaction contributes substantially to the overall rate of reaction. In detail, mass transfer limitations occur on the surface of the catalyst because the reaction proceeds *via* a liquid–liquid–solid stage [2, 24]. Therefore, by creating a CaO surface that is easily accessible to both methanol and oil, reductions in mass transfer limitation could be achieved [2, 6, 8, 17]. In addition, as mentioned previously, a combination of SSA increase with an increase in the basicity of the catalyst would also serve to improve the rate of methanolysis.

To our knowledge, the derivation of a CaO catalyst from scallop shell and subsequent activation by a methanol-assisted dry nano-grinding process has not been previously reported. In this study, we examined the use of CaO-ss as a catalyst for the methanolysis of soybean oil, and we report the effects of active phase surface composition on the initial rate of reaction, as well as the effects of the oxide's SSA.

## 2. Experimental

### 2.1 *Dry nano-grinding process and catalyst characterization*

CaO-ss (SSA = 0.4 $m^2g^{-1}$) was obtained from the calcination of scallop shell powder at 1000 °C for 3 h. The methanol-assisted dry nano-grinding process was carried out using a planetary ball mill (P-7 premium line, Fritsch, Germany), which was equipped with two zirconia pots of 80 $cm^3$ volume, each containing 100 g of yttria-stabilized zirconia milling beads (3 mm diameter). To evaluate the grinding process, experiments involving batchwise and stepwise addition of methanol were carried out in a closed system. The batchwise addition method was performed by adding the whole required volume of methanol into the pot at the start of the nano-grinding process, whereas the stepwise addition method involved adding smaller

quantities of methanol to the pot at predetermined intervals. During batchwise addition, the nano-grinding operation was stopped for 15 min after every 1 h of grinding to prevent the inside of the milling pot from overheating. After a predetermined grinding time, the ground mixture was removed. The range of different conditions used in the nano-grinding process is shown in **Table 1**.

The SSA of the powders was determined from nitrogen gas adsorption by using the five-point BET method (Microtrac, Adsotrac DN-04). Prior to measurement, samples were degassed at 473 K for 2 h.

X-ray powder diffraction (XRD) measurements were performed by a Multi Flex-120 NP Rigaku (Japan) equipped with a Cu-Kα anode (λ = 1.5418 Å), operated at a tension and current of 40 kV and 20 mA, respectively. Measurements were recorded at room temperature over the 2θ range 3–70°, with a 0.02° step size. Crystalline phases were identified by comparison with ICDD data files.

Fourier-transform infrared (FTIR) spectra were recorded using a JASCO FTIR-460 PlusK spectrometer, and catalyst was measured as KBR pellets. Measurements were conducted over the range 4000–400 $cm^{-1}$ with a 4 $cm^{-1}$ resolution.

Total basic sites ($f_m$) of the catalysts were evaluated by measuring the acidity conjugate acid, by titration method. In a typical experiment, 25 mg catalyst of ground CaO was dissolved in 25 mL of 0.1 M HCl and resulting mixture was stirred for 1 hour. The catalyst would neutralize HCl equivalent to its basicity. The resulted solution was titrated against standard NaOH solution to determine the exact concentration of excess HCl. The amount of HCl neutralized by the catalyst was determined and represented as basicity of the catalyst as mmol of HCl/g of catalyst [25].

## 2.2 *Methanolysis of soybean oil*

The effect of SSA and surface phase composition on the initial reaction rate of methanolysis reaction was tested. Methanolysis of soybean oil was performed in a 100 mL batch-type three-necked glass flask with a condenser and magnetic stirrer. The transesterification was carried out at 65±1 °C with a methanol-to-oil molar ratio of 9:1 and catalyst concentration of 4 wt% with respect to the oil mass. The stirring rate was held at 800 rpm. A series of CaO-ss samples with the following SSA: 0.4 $m^2g^{-1}$; 4.5 $m^2g^{-1}$; 10.6 $m^2g^{-1}$; 17.3 $m^2g^{-1}$; 18.6 $m^2g^{-1}$; 25.9 $m^2g^{-1}$; 27.9 $m^2g^{-1}$; 31.0 $m^2g^{-1}$; 35.6 $m^2g^{-1}$; 45.2 $m^2g^{-1}$; 45.3 $m^2g^{-1}$; 45.6 $m^2g^{-1}$; 46.3 $m^2g^{-1}$; 57.4 $m^2g^{-1}$; 62.5 $m^2g^{-1}$ were used. Prior to analysis, samples (1 ml) were removed from the reaction

mixture and immediately treated using a procedure detailed elsewhere [26]. The quantities of esters, monoglyceride, diglyceride, and triglyceride were analyzed using a gas chromatograph (Shimadzu GC-14B) equipped with a flame ionization detector (FID), on a DB-5HT capillary column (14 m × 0.25 mm, 0.1 μm film thickness). The analytical work was performed with the following heating regime: holding at 50 °C for 1 min, followed by three separate steps of temperature increase, firstly to 180 °C at a rate of 10 °C/min, then to 230 °C at 7 °C/min, and lastly to 380 °C at 10 °C/min, at which point the temperature was held for 10 mins. Quantitative analysis was carried out following a procedure described in detail elsewhere [27]. To examine the catalyst recyclability, the spent catalyst was used five separate times through recovery by filtration, washing with acetone, and drying in a vacuum at room temperature.

**Table 1**

Methanol assisted dry nano-grinding conditions

| Entry | Catalyst preparation |
|---|---|
| 1 | Calcinated scallop shells at 1000 °C for 3 h. |
| 2 | Nano-grinding with 0.2 ml methanol at 400 rpm, 3 h. Batchwise addition. |
| 3 | Nano-grinding with 1 ml methanol at 1000 rpm, 30 min. Batchwise addition. |
| 4 | Nano-grinding with 3 ml methanol at 1000 rpm, 5 h. For stepwise addition, solvent added at rate of 0.6 ml/1 h. |
| 5 | Nano-grinding with 1 ml methanol at 1000 rpm, 4 h. Batchwise addition. |
| 6 | Nano-grinding with 1.8 ml methanol at 400 rpm, 6 h. For stepwise addition, solvent added at rate of 0.3 ml/1 h. |
| 7 | Nano-grinding with 0.45 ml methanol at 400 rpm, 6 h. For stepwise addition, solvent added at rate of 0.075 ml/1 h. |
| 8 | Nano-grinding with 3 ml methanol at 400 rpm, 10 h. Batchwise addition. |
| 9 | Nano-grinding with 4.5 ml methanol at 1000 rpm, 6 h. For stepwise addition, solvent added at rate of 0.75 ml/1 h. |
| 10 | Nano-grinding with 3.75 ml methanol at 900 rpm, 5 h. For stepwise addition, solvent added at rate of 0.75 ml/1 h. |
| 11 | Nano-grinding with 3 ml methanol at 1000 rpm, 5 h. For stepwise addition, solvent added at rate of 0.6 ml/1 h. |
| 12 | Nano-grinding with 3 ml methanol at 1000 rpm, 5 h. For stepwise addition, solvent added at rate of 0.6 ml/1 h. |
| 13 | Nano-grinding with 1.8 ml methanol at 600 rpm, 6 h. For stepwise addition, solvent added at rate of 0.3 ml/1 h. |
| 14 | Nano-grinding with 4.5 ml methanol at 400 rpm, 3 h. For stepwise addition, solvent added at rate of 0.5 ml/20 min. |

| | |
|---|---|
| 15 | Nano-grinding with 0.9 ml methanol at 600 rpm, 6 h. For stepwise addition, solvent added at rate of 0.3 ml/2 h. |

## 3. Result and discussion

### 3.1 *Bulk and surface characterization of catalysts*

**Table 2** presents the variations in the SSA of the ground CaO-ss samples after being processed by methanol-assisted dry nano-grinding. As can be seen, the variations of SSA (4.5–62.5 $m^2g^{-1}$) were determined by a number of nano-grinding parameters: batchwise or stepwise addition of solvent; rotation of milling; grinding time with the various volumes (0.2–4.5 ml) of methanol. The presence of methanol in the nano-grinding process is thought to protect the particles from agglomeration: with a sufficient concentration of methanol, the formation of terminal methoxide groups, as opposed to bridging, is promoted; terminal methoxy groups act to hinder inter-particle bonding which is known to lead to formation of hard agglomerates. Similar behavior has been observed by other authors [28, 29] in organic solvent-assisted dry grinding processes. Reducing both the attractive forces between particles, as well as adhesion to the grinding media have the effect of improving the 'grindability' of the oxide which, in turn, produces material with higher SSA.

The temperature of the nano-grinding pot during processing was measured to be between 60 °C and 120 °C for batchwise addition, and between 60 °C and 80 °C for stepwise addition. As these temperatures were higher than the boiling point for methanol, CaO-ss was ground in methanol vapor. Comparing the batchwise and stepwise addition methods, the latter was found to be effective for obtaining higher SSA CaO-ss (**Table 2**). This may be explained by considering the high volatility of methanol in the vapor phase: in batchwise addition, the volatility of methanol leads to insufficient adsorption to the catalyst surface to produce the protective effect. While quantifying the effects of methanol volatility and adsorption to CaO-ss is beyond the scope of this study, the results suggest that stepwise addition can maintain the methanol vapor concentration at a sufficient level to shield the particle surface, as evidenced by the improvements in grindability and SSA.

In previous reports, it has been revealed that the nano-grinding process could promote chemisorption and physisorption reactions on the surfaces of solid particles. [28, 30]. The changes in the relative proportions of active phases on the surface of ground CaO-ss (which is associated with the adsorption of methanol vapor) were evaluated by XRD and FT-IR measurements. The XRD patterns of CaO-ss catalysts, treated as listed in **Table 1**, are shown in **Fig. 1 (a)-(c)**. The XRD results confirmed that a number of different calcium-based phases are formed during the methanol-assisted dry nano-grinding process. The crystalline phases were indexed and

matched to three known materials: calcium oxide (ICDD file 04-1497), calcium hydroxide (ICDD file 04-0733), and calcium methoxide (reported in [26]). The presence of active sites on the ground CaO-ss catalyst modified the basicity of the catalysts as shown in **Table 2**.

The FT-IR results are summarized in the Supporting Information **Fig. S2**: from these results, it can be inferred that methanol vapor adsorption during the nano-grinding stage occurs *via* both chemisorption and physisorption pathways. The interaction between CaO-ss and methanol begins with the adsorption of the vapor onto the oxide surface. The adsorbed methanol can then either desorb or dissociate during the nano-grinding process. In all of the ground CaO-ss samples, sharp bands at 3643 $cm^{-1}$ were observed in the O-H stretching vibration region $\nu$ (OH) of CaO-H on the ground CaO-ss surface [31]. This indicates that dissociation of methanol at the catalyst surface proceeds via hydrogen bonding between the methanol H and the surface O atoms of CaO-ss. These results roughly agree with results reported elsewhere, which signify that methanol vapor decomposition proceeds by O-H bond scission [32, 33, 34]. The methoxide groups were identified by the presence of a couple of weak bands in the C-H stretching region at 2925 $cm^{-1}$ and 2831 $cm^{-1}$ and in the C-H deformation region (1500–1400 $cm^{-1}$), attributed to the $\delta$(CH) modes of methoxide. This suggests that interactions between methoxide groups and the CaO surface arises *via* the lone pair of electrons on the oxygen atom [33]. In the C-O stretching (primary alcohol) region, bands in the range 1148–1078 $cm^{-1}$ were present, which correspond to $CH_3O^-$ groups [28, 32, 36]. The weak peak present in the region 865–875 $cm^{-1}$ was attributed to $CO_2$ adsorbed on the CaO-ss surface [21, 31].

A shoulder at 3229 $cm^{-1}$ and 3300–3400 $cm^{-1}$ was also detected and assigned to H-bonds, which form on dissociative adsorption of methanol, while the band at 3300–3500 $cm^{-1}$ was linked to the –OH mode of water physisorption on the CaO-ss surface [33, 35], and the detection of a band in the region 1650–1600 $cm^{-1}$ was assigned to the H-O-H deformation water molecules physisorbed on the catalyst surface [31]. In this work, the overlapping of this region band occurred for the CaO-ss samples 2–6, 8–10, 12, and 14–15. Taking FT-IR bond scission features as references, a possible reaction mechanism for methanol adsorption during nano-grinding is proposed as follows:

$$CaO \leftrightarrow Ca^{2+} + O^{2-} \quad (1)$$

$$CH_3OH_{(g)} \rightarrow (CH_3OH)_{(a)} \quad (2a)$$

$$CH_3OH_{(a)} \rightarrow CH_3O^-_{(a)} + H^+_{(a)} \quad (2b)$$

$$Ca^{2+} + 2CH_3O^-_{(a)} \rightarrow Ca(OCH_3)_{2\,(a)} \quad (3a)$$

$$Ca^{2+}\text{-}O^{2-} + H^+_{(a)} \rightarrow Ca^{2+}\text{-}O^{2-}\text{-}H^-_{(a)} \quad (3b)$$

$O^{2-} + 2H^-_{(a)} \rightarrow H_2O_{(a)}$ (3c)

$Ca\text{-}O + H_2O_{(a)} \rightarrow Ca(OH)_{2\,(a)}$ (3d)

$Ca^{2+}\text{-}\ O^{2-}\text{-}H^- + H^-\text{-}\ O^{2-}\text{-}\ Ca^{2+} \rightarrow Ca\text{-}O\text{-}Ca + H_2O$ (4)

* (a) = adsorbed."

As we mentioned previously, the stepwise addition method was found to be more effective for obtaining high SSA CaO-ss. Grinding-induced activation of CaO produced surface ions ($Ca^{2+}$ and $O^{2-}$) but the overall crystal is neutral (1) [28]. Interactions between methanol vapor and these surface ions occurred via chemisorption and physisorption (**Fig. 2(a),(b)**) during the nano-grinding process. Therefore, several calcium-based phases were generated at the catalyst surface, namely calcium oxide, calcium hydroxide, and calcium methoxide (**Fig. 3(a)-(d)**) as shown in **Fig. 1 (a)-(c)**. The calcium methoxide phases also act to protect the particulates from agglomeration (**Fig. 2(a)** and **3(a)**): the lower the agglomeration energy, the smaller the agglomerated particles which form during the process, thereby yielding a higher SSA product [37]. Because the methanol vapor adsorbed weakly at the temperatures produced by the nano-grinding process (60–120 °C), the stepwise addition method is more effective in maintaining a sufficient concentration of methanol vapor during grinding, and therefore this variation of the process yielded higher SSA CaO-ss.

Water physisorption on the ground CaO-ss surface was also identified, as shown in Supporting Information as **Fig. S2**, probably arising due to non-bridging hydroxyl groups tend to interact strongly on the ground CaO-ss surface, which liberates water (4). Consequently, hard agglomerates formed, which reduced the SSA of the products.

Summarizing the FT-IR results, it can be concluded that methanol-assisted dry nano-grinding with stepwise solvent addition is very effective in increasing the SSA of CaO-ss catalysts, and the addition of methanol to the nano-grinding process also serves to generate several active phases on the surface of the catalysts.

**Table 2**

CaO-ss prepared samples: SSA and XRD Characterization

| Entry | SSA ($m^2g^{-1}$) | Crystalline phases* | Basicity (mmoles of HCl/g of catalyst) | Esters yield (%) 20 min reaction | Esters yield (%) 60 min reaction |
|---|---|---|---|---|---|
| 1 | 0.4 | **CaO** | 0.16 | 13.7 | 16.1 |
| 2 | 4.5 | **CaO** | 0.19 | 34.8 | 81.7 |
| 3 | 10.6 | **$Ca(OH)_2$**, CaO | 0.22 | 44.4 | 92.1 |
| 4 | 17.3 | **$Ca(OCH_3)_2$** CaO, $Ca(OH)_2$ | 0.22 | 29.8 | 83.8 |
| 5 | 18.6 | **CaO**, $Ca(OH)_2$ | 0.22 | 46.2 | 95 |
| 6 | 25.9 | **CaO**, $Ca(OH)_2$, $Ca(OCH_3)_2$ | 0.26 | 50.8 | 94.7 |
| 7 | 27.9 | CaO, **$Ca(OH)_2$**, $Ca(OCH_3)_2$ | 0.35 | 58.9 | 97.5 |
| 8 | 31 | **$Ca(OCH_3)_2$** CaO, $Ca(OH)_2$ | 0.22 | 41.2 | 95.6 |
| 9 | 35.6 | **$Ca(OH)_2$**, $Ca(OCH_3)_2$ | 0.22 | 57.6 | 95.7 |
| 10 | 45.2 | **CaO**, $Ca(OH)_2$, $Ca(OCH_3)_2$ | 0.29 | 72.3 | 96.5 |
| 11 | 45.3 | **$Ca(OH)_2$** | 0.19 | 37.6 | 94 |
| 12 | 45.6 | **$Ca(OH)_2$** | 0.19 | 39.5 | 95.7 |
| 13 | 46.3 | $Ca(OH)_2$, **$Ca(OCH_3)_2$** | 0.22 | 45.5 | 93.5 |
| 14 | 57.4 | **$Ca(OH)_2$**, $Ca(OCH_3)_2$ | 0.22 | 50 | 91 |
| 15 | 62.5 | **$Ca(OH)_2$** | 0.22 | 53.7 | 96.5 |

*Phases highlighted in bold indicate major phases observed by XRD analysis.

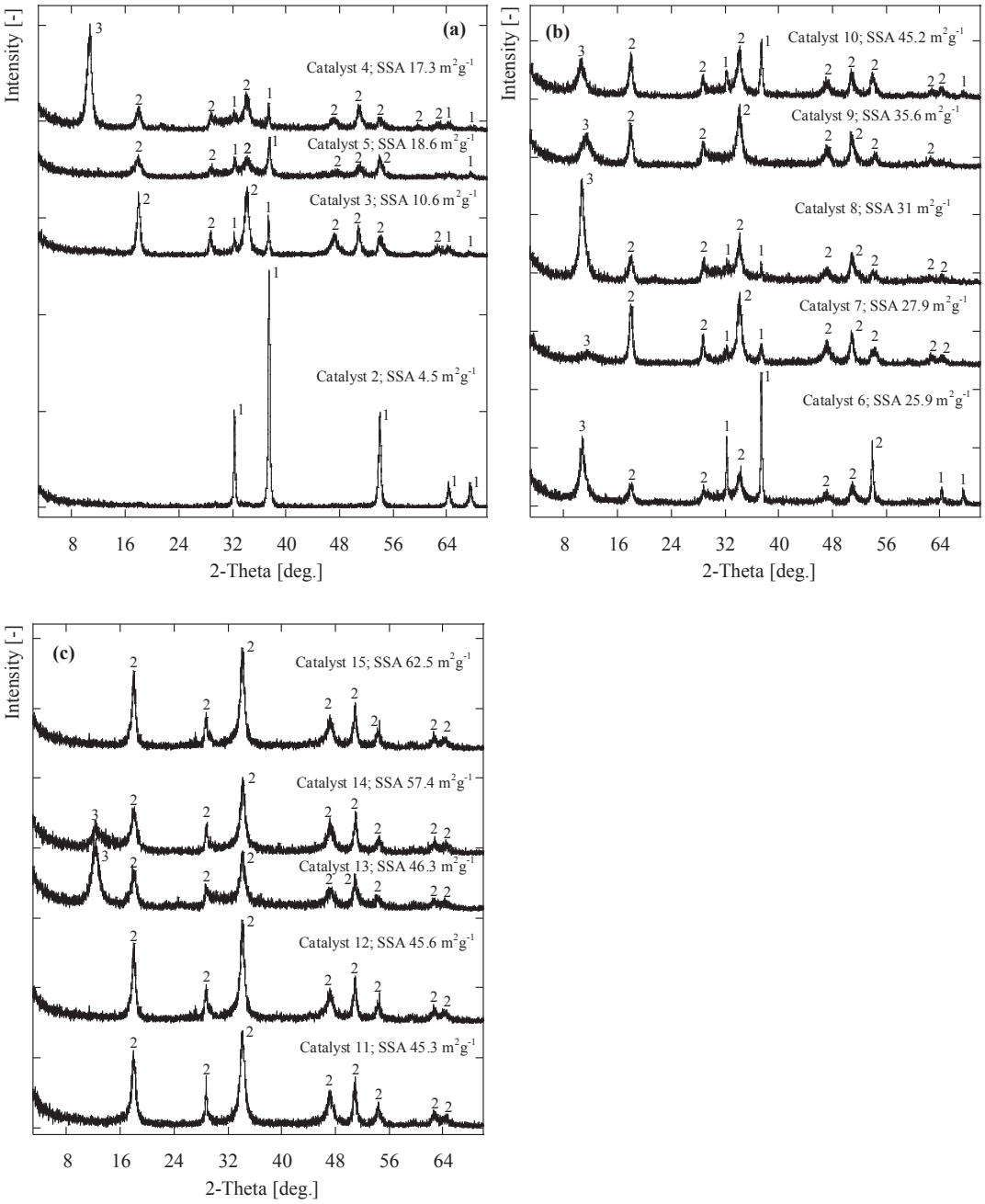


**Fig. 1**. XRD patterns of ground CaO-ss after processing by methanol-assisted dry nano-grinding; (1) CaO, ICDD file 04-1497; (2) $Ca(OH)_2$, ICDD file 04-0733; (3) $Ca(OCH_3)_2$ refer to [26].

### 3.2 *Methanolysis of soybean oil*

As many studies have reported, the reaction rate of heterogeneous methanolysis reaction rate is predominantly determined by both mass transfer and the surface reaction, but the limitations of mass transfer limitations are slightly more significant than those of the reaction [2, 36, 38]. Therefore, in order to improve the overall rate, the mass transfer limitations present in the initial stages of the methanol–oil–solid catalyst system needs to be reduced first. The results of methanolysis reactions using the CaO-ss catalysts are presented in **Fig. 2 (a)** and **(b)**, showing that the catalytic activity of the ground CaO-ss is much higher compared to untreated CaO. Under the reaction conditions detailed in the Methods section, ester yields in the range of 29.8–72.3% were obtained. On increasing the catalyst SSA from the lowest value of 0.4 $m^2g^{-1}$, the rate of methanolysis was observed to increase drastically (**Table 2**). These faster reaction rates can be ascribed to the improved access of reactant molecules to basic sites at surface of the ground CaO-ss catalyst, which arises from the increase in surface area. Additionally, the high SSA values associated with nanoscale crystallite sizes provide shorter paths for reactant to surface of the catalyst, which also reduces the mass transfer limitations [2]. On decreasing the mass transfer limitations, the surface reaction rate subsequently increased, leading to a distinctly increased overall rate of reaction and decreased reaction time.

The Koras-Nowak criterion test was conducted to assess whether the measured CaO catalyst ground catalytic activity was independent of the influence of transport phenomena [39]. Similar to previous report in [25], the reaction was conducted on two catalysts, Entry 12 and Entry 15 with different SSA but same active phases ($Ca(OH)_2$). In a typical test, with similar fractional exposures of basic sites but having different SSA. In present study, 2 wt% of Entry 12 and or 4 wt% of Entry 15 catalyst dosages was applied at 65±1 °C with a methanol-to-oil molar ratio of 12:1 or methanol-to-oil molar ratio of 9:1. Samples were taken every 5 min, then were analyzed by GC. When the conversion of the soybean oil was the same, the reaction recorded. The results exhibited in **Fig. 3** showed that the turnover frequency (TOF) on the two catalysts were nearly the same with the same conversion, thus indicated that the reaction obeyed the Koras-Nowak criterion.

**Figure 2 (a)** and **(b)** also show that the reaction rate did not increase directly proportionally to the SSA, as was expected. For example, in the case of catalysts 6 and 12 (**Table 1**), the former produced an ester yield of 50.8% with a SSA of 25.9 $m^2g^{-1}$, whereas the latter only produced an ester yield of 39.5%, despite possessing an SSA of 45.6 $m^2g^{-1}$. The XRD pattern of the lower SSA catalyst 6 indicated that calcium oxide was present as the major phase along with significant quantities of

calcium methoxide, whereas the diffraction peak arising from calcium hydroxide was small. In contrast, catalyst 12 (higher SSA) was observed by XRD to contain only calcium hydroxide. This implies that the active phases on the catalyst surface played a crucial role in determining catalytic activity of the ground CaO-ss during the methanolysis reaction. Since the reaction occurs on the surface of the catalyst, the number of accessible basic sites, the basicity of those sites, and the rate of mass transfer to them determine the reaction rate (**Table 2**). Analogous results have been published by Kouzu *et al.*, who reported that calcium hydroxide was much less active in the methanolysis of soybean oil than calcium oxide. The authors ascribed the lower catalytic activity to the differing basicity of the catalysts [18].

Surprisingly, catalysts 3, 5–7, 10, 13, and 14 exhibited higher ester production: yields between 44% and 72% were achieved at 20 min, while yields of 92–97% were achieved at 1 h for all samples (**Table 2**). From the XRD patterns (**Fig 1 (a)-(c)**) and FT-IR spectra (IR bands at 3643 $cm^{-1}$ and 3300–3500 $cm^{-1}$, **Fig. S2**), all of these ground CaO-ss catalysts were found to contain calcium hydroxide on their surfaces, which would be expected to hinder the methanolysis. We attribute their high performance to a faster rate of methoxide anion generation via surface $OH^-$ which initiates the methanolysis reaction [14, 40, 41]. These results are in good agreement with previous reports, which assert that neighboring hydroxyl groups (formed by methanol-assisted dry nano-grinding) modify the basic strength of the $Ca^{2+}$–$O^{2-}$ pair, which methanol adsorbs onto directly prior to methoxide anion generation. The methoxide anion then forms a tetrahedral intermediate, and thus is a key component in the initiation of the transesterification reaction. Although physisorbed water molecules were detected on the surface of catalysts 3, 5–7, 10, 13, 14 (IR bands at 1650–1600 $cm^{-1}$), these seemingly acted as Bronsted basic sites for methanol activation [40]. On the other hand, the activities of catalysts 11, 12, and 15 showed a low rate of methanolysis—ester yield of 37–54% achieved after 20 min—most likely owing to their complete conversion to calcium hydroxide (**Fig. 1 (c)**): these results agree with the previously published reports [15, 16]. From these results, we can conclude that the catalytic activity of ground CaO-ss is determined not only by SSA but also by its basicity, and that the presence of high quantities of calcium hydroxide hinders the performance of the catalysts. **Figure 4** shows a possible mechanism for transesterification catalyzed by the ground CaO-ss with its active phases. Methanol and triglyceride are adsorbed on several neighboring free of CaO-ss catalytic sites ($O^-$, $OH^-$, $Ca^{2+}$). Surface $O^-$ and $OH^-$, extracts an $H^+$ and $Ca^{2+}$ adsorbs $CH_3O^-$ from $CH_3OH$ to form $CH_3O^-$ and $H^+$ on the surface. The adsorbed triglyceride forms a surface intermediate. The two neighboring adsorbed species react to result in the formation of fatty acid methyl ester and diglyceride. The diglyceride reacts with methanol along

the similar processes on the surface of catalyst to form glycerol and esters.

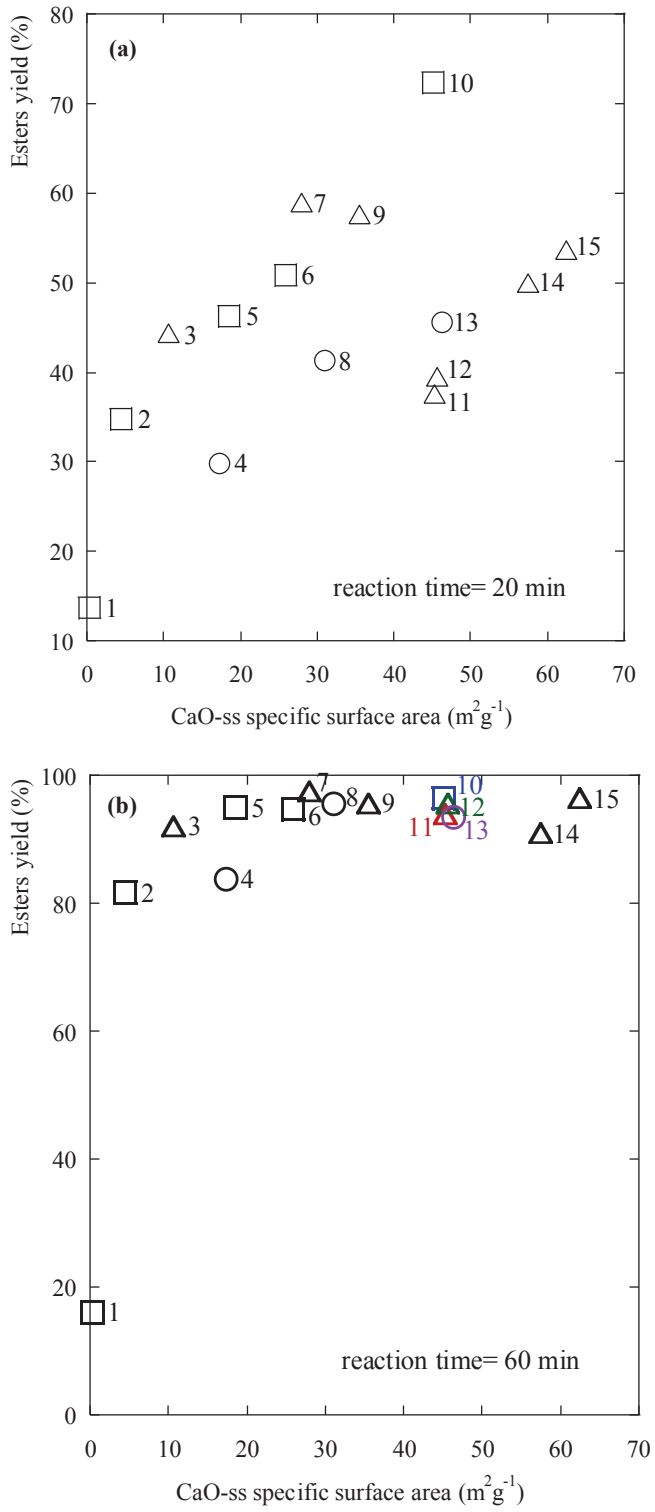


**Fig. 2**. Plot correlating the ester yield of heterogeneous methanolysis with the specific surface area and active phases of the ground CaO-ss catalyst for **(a)** 20 min **(b)** 60 min reaction times.

Square denotes that calcium oxide active phase is present; triangle denotes that calcium hydroxide active phase is present; circle denotes calcium methoxide active phase is present. Numbers indicate catalysts number (see **Table 2**).

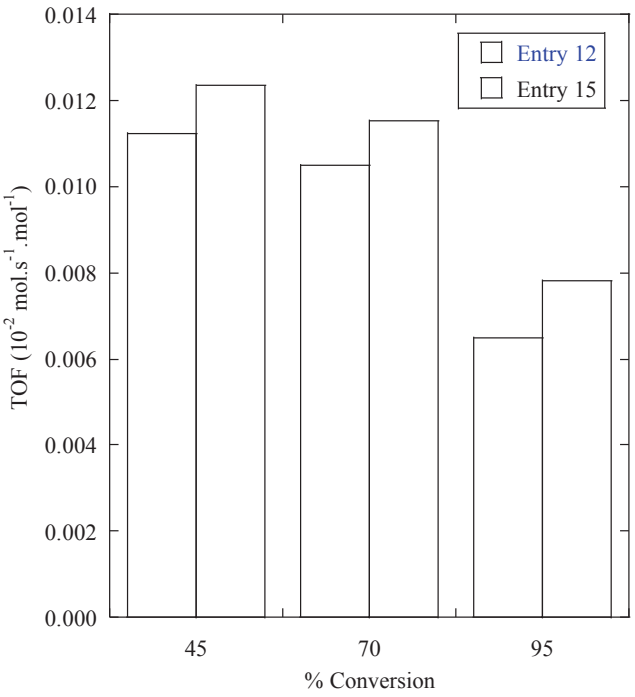


**Fig. 3**. TOF of 2 wt% of Entry 12 and or 4 wt% of Entry 15 catalyst dosages was applied at 65±1 °C with a methanol-to-oil molar ratio of 12:1 or methanol-to-oil molar ratio of 9:1.

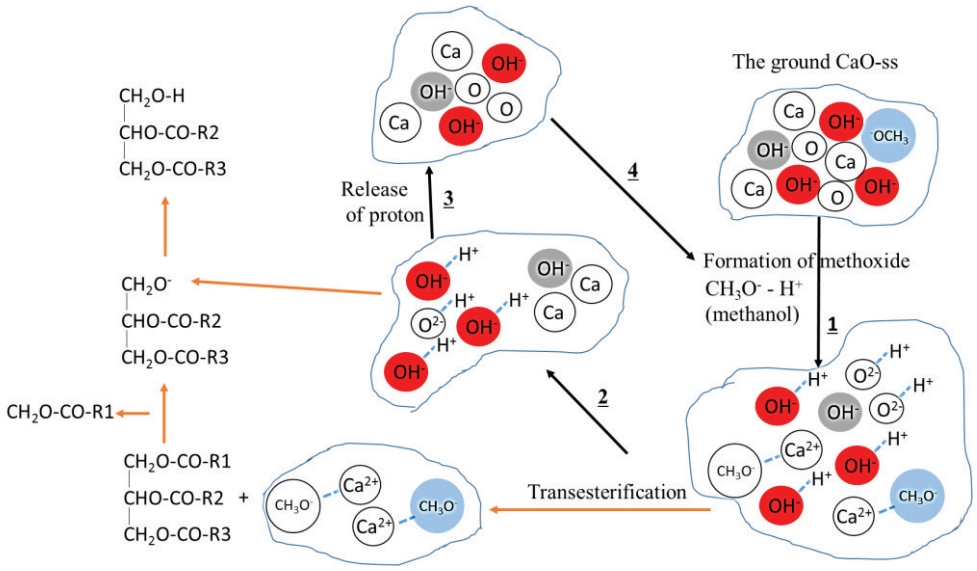


**Fig. 4** A proposed mechanism for transesterification catalyzed by the ground CaO-ss

with its active phases. ($OH^-$) in red is hydroxyls from partially transformed to $Ca(OH)_2$, ($OH^-$) in grey is hydroxyls from totally transformed to $Ca(OH)_2$, $CH_3O^-$ in blue is methoxide from partially transformed to Ca-methoxide on the ground CaO-ss surface.

It has been previously reported that calcium methoxide has a higher basic strength and higher catalytic activity during methanolysis compared to CaO and $Ca(OH)_2$ [5, 24, 26, 36]. The results in this work do not show this trend; catalysts 4 and 8 (calcium methoxide as the major active phase) displayed a lesser degree of activity compared to catalysts 5 and 6 (calcium oxide being the dominant phase) (**Table 2**). A plausible explanation for this relates to the strong bonding between the calcium methoxide phase and the bulk catalyst. This behavior would result in slower nucleophilic attack on the triglyceride carbonyl carbon to yield a tetrahedral intermediate, which starts the methanolysis reaction. As mentioned above, the rate of CaDg formation is an indication of the degree of mass transfer limitation in the system. In an attempt to assess the structural strength of the calcium methoxide active phase bonded to the bulk catalyst, XRD was used to identify the point at which the catalyst structure converts to CaDg. **Figure 5 (a)** and **(b)** shows the XRD patterns of CaO-ss 4 and 8 prior to reaction and at 10 min, 20 min, and 60 min of reaction. The patterns were fingerprinted using the calcium oxide phase (ICDD file 04-1497), calcium hydroxide phase (ICDD file 04-0733), calcium methoxide reported in [26], and CaDg reported in [42]. The SSA of catalysts 4 and 8 were measured to be 17.3 $m^2g^{-1}$ and 31 $m^2g^{-1}$, respectively. According to Esipovich *et al.*, CaDg can form through interaction with $Ca^{\delta+}$ and $CH_3O^{\delta+}$ groups: the surface $CH_3O^{\delta+}$ extracts H from glycerol and $Ca^{\delta+}$ adsorbs glyceroxide [7]. From the XRD patterns of used catalyst 4, the active calcium methoxide phase was shown to be present, even after 60 mins of reaction. The enhancement in SSA of the catalyst from 17.3 $m^2g^{-1}$ to 31 $m^2g^{-1}$ in catalyst 8 with reference to the XRD patterns in **Figure 4 (a) and (b)** identifying which features indicate that calcium methoxide to CaDg conversion occurs more rapidly. Hence, the higher SSA of the catalyst contributed to lowering mass transfer limitations during the initial stages of the reaction.

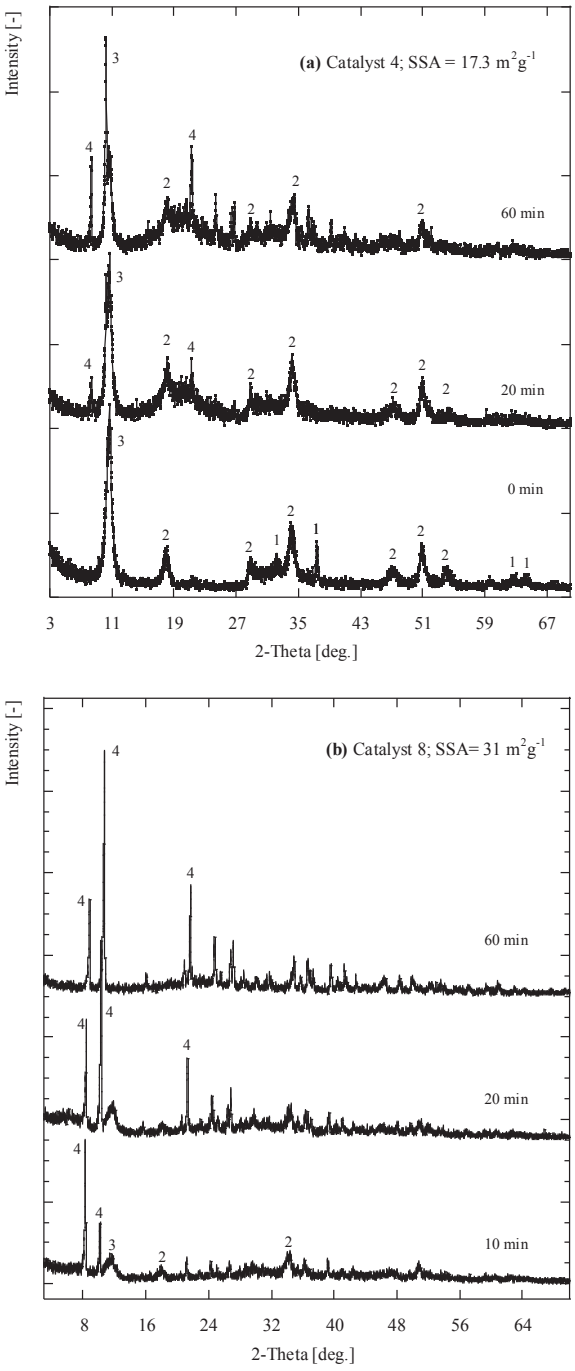


**Fig. 5**. XRD patterns of used catalysts collected after taking part in the heterogeneous methanolysis reaction: (a) catalyst 4, and (b) catalyst 8. (1) CaO, ICDD file 04-1497; (2) $Ca(OH)_2$, ICDD file 04-0733; (3) $Ca(OCH_3)_2$ was taken from [26]; CaDg was taken from [42].

To study the role of SSA and active phases (**Fig. 2**) in reducing mass transfer limitations in the methanolysis of soybean oil, we also investigated chemical changes in the catalysts during the reaction. It has previously been reported that the presence of CaDg predominantly affects the initial stage of the methanolysis reaction [17]: CaDg promotes the mutual miscibility of triglycerides and methanol, increasing the area of the liquid–solid interface (the liquid component consisting of triglycerides in the methanol phase), which, in turn, increases the overall methanolysis rate. Additionally, another study concluded that CaO only acts as an active phase at the beginning of the reaction, while CaDg is believed to be the 'true' active phase in CaO-catalyzed methanolysis [18].

The results of this investigation show that the presence of active phases at the surface of high SSA CaO-ss catalysts play a determining role in reducing mass transfer limitations during the initial stages of reaction. From this, it is evident that active phases can modify the basicity of the catalysts to either stronger or weaker degrees, which mostly occurs in the case of calcium hydroxide.

Taking the case of catalyst 10 and Entry 12 (**Table 2**), we can investigate the effects of the presence of the active calcium hydroxide phase. The SSA of catalyst 10 was 45.2 $m^2g^{-1}$, and 45.6 $m^2g^{-1}$ for catalyst 12, producing ester yields of 72.3% and 39.5%, respectively. Although measurement of catalyst basicity was not conducted in this work, it can be inferred from the results that the active calcium hydroxide phase on the surface of catalyst 10 was able to modify and enhance the surface basicity, whereas the calcium hydroxide phase on the surface of catalyst 12 did not show the same behavior. The XRD patterns (**Fig. 1 (b)** and **(c)**) showed that a $Ca(OH)_2$ peak was visible in catalyst 10, but the bulk had not been fully transformed to $Ca(OH)_2$; on the other hand, catalyst 12 was observed to have undergone a full transformation to $Ca(OH)_2$. The activity of these two catalysts can be evaluated by comparing the time of CaDg formation in the methanolysis reaction. **Figure 5 (a)** and **(b)** show rapid formation of CaDg formation on catalyst 10 during the first 10 min of the reaction; in contrast, CaDg was only observed to form on catalyst 12 after 60 mins. This reiterates that CaDg is important not only for improving the miscibility between methanol and oil, but also, as previous authors have reported, as a highly active phase during the heterogeneous methanolysis reaction [17, 42].

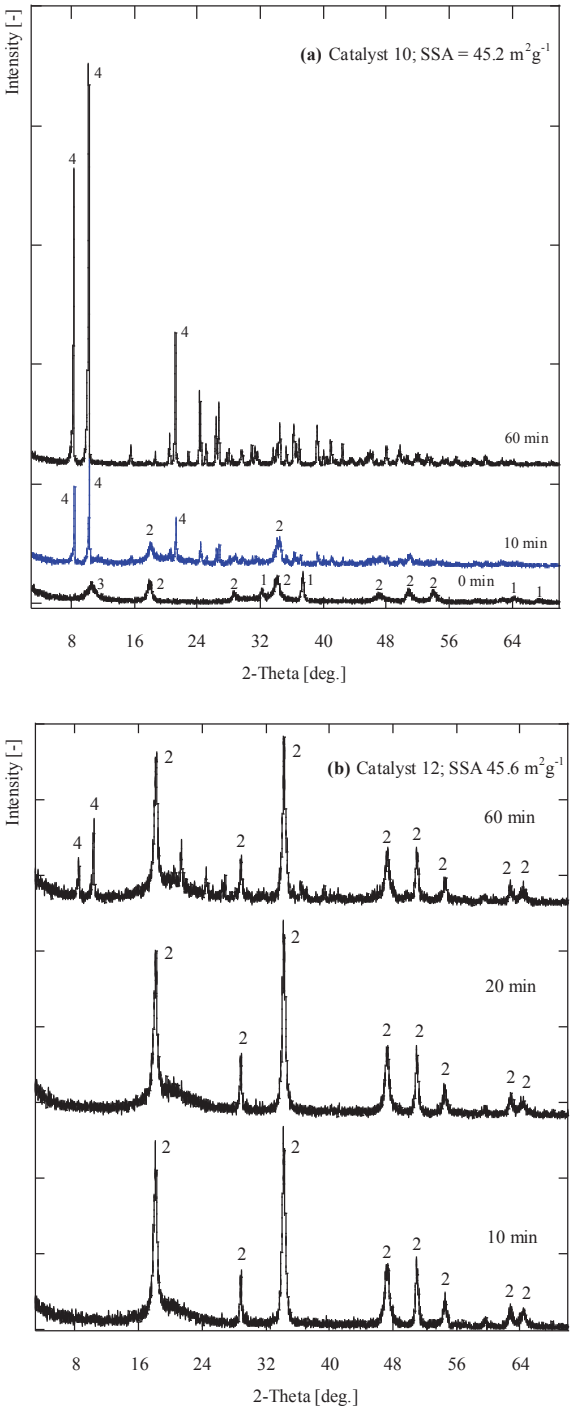


**Fig. 6**. XRD patterns of the used catalysts collected from the heterogeneous methanolysis reaction for (a) used catalyst 10, and (b) used catalyst Entry 12. (1) CaO, ICDD file 04-1497; (2) $Ca(OH)_2$, ICDD file 04-0733; (3) $Ca(OCH_3)_2$ refer to [26]; CaDg refer to [42].

## 4. Conclusions

The SSA of CaO-ss was successfully enhanced by methanol-assisted dry nano-grinding. Characterization of CaO-ss after nano-grinding showed that this process could generate three different calcium-based phases on the oxide surface: calcium oxide, calcium methoxide, and calcium hydroxide. These active phases behave differently during methanolysis, and they were observed to modify the basicity of the catalyst surface, which can affect the overall reaction rate. The highest catalytic activity in a heterogeneous methanolysis reaction was observed for CaO-ss samples that had undergone partial surface conversion to $Ca(OH)_2$.

These results show that the combination of a high SSA and an optimal active phase surface composition of the catalyst can be highly effective in suppressing the mass transfer limitations during the initial stage of the methanolysis reaction. High SSA, nanosized particles provide a large number of accessible reaction sites and shorter paths for reactant to surface of the ground CaO-ss, while specific active phases simultaneously enhanced the basic strength of the catalysts. This behavior has an important role at the beginning of the methanolysis reaction as it strongly affects the formation of CaDg, which not only improves miscibility of oil and methanol, which reduces mass transfer limitations, but also actively catalyzes the heterogeneous methanolysis reaction. The reduction in CaDg formation time during the early stages of the reaction was an important effect arising from the combination of high SSA and effective active phase composition on the catalyst surface.

## References


[1] R. Wang, H. Li, F. Chang, J. Luo, M.A. Hanna, et al, A facile, low-cost route for the preparation of calcined porous calcite and dolomite and their application as heterogeneous catalysts in biodiesel production, Catal. Sci. Technol. 3 (2013) 2244-2251.

[2] L. Zhao, Z. Qiu, S.M. Stagg-Williams, Transesterification of canola oil catalyzed by nanopowder calcium oxide, Fuel Processing Technology 114 (2014) 154-162.

[3] S. H. Teo, Y. H. Taufiq-Yap, U. Rashid, A. Islam, Hydrothermal effect on synthesis, characterization and catalytic properties of calcium methoxide for biodiesel production from crude *Jatropha curcas*, RSC Adv. 5 (2015) 4266-4276.

[4] A. N. R. Reddy, A. A. Saleh, Md. S. Islam, S. Hamdan, Md. A. Maleque, Biodiesel production from crude Jatropha oil using highly active heterogeneous nanocatalyst by optimizing transesterification parameters, Energy Fuels 30 (2016) 334-343.

[5] D. Cornu, H. Guesmi, G. Laugel, J. M. Krafft, H. Lauron-Pernot, On the relationship between the basicity of a surface and its ability to catalyze transesterification in liquid and gas phases: the case of MgO, Phys. Chem. Chem. Phys. 17 (2015) 14168-14176.

[6] C. R. V. Reddy, R. Oshel, J. G. Verkade, Room-temperature conversion of soybean oil and poultry fat to biodiesel catalyzed by nanocrystalline calcium oxides, Energy & Fuels 20 (2006) 1310-1314.

[7] A. Esipovich, S. Danov, A. Belousov, A. Rogozhin, Improving methods of CaO transesterification activity, J. of Molecular Catalysis: Chemical 395 (2014) 225-233.

[8] D. Cornu, H. Petitjean, G. Costentin, H. Guesmi, J. M. Krafft, H. Lauron-Pernot, Influence of natural adsorbates of magnesium oxide on its reactivity in basic catalysis, Phys. Chem. Chem. Phys. 17 (2013) 19870-19878.

[9] M. Kouzu, S. Yamanaka, J. Hidaka, M. Tsunomori, Heterogeneous catalysis of calcium oxide used for transesterification of soybean oil with refluxing methanol, Applied Catalysis A: General 355 (2009) 94-99.

[10] K. Wilson, C. Hardacre, A. F. Lee, J. M. Montero, L. Shellard, The application of calcined natural dolomitic rock as a solid base catalyst in triglyceride transesterification for biodiesel synthesis, Green Chem. 10 (2008) 654-659.

[11] A. Buasri, N. Chaiyut, V. Loryuenyong, P. Worawanitchaphong, S. Trongyong, Calcium oxide derived from waste shells on mussel, cockle, and scallop as the heterogeneous catalyst for biodiesel production, Sci. World J. 2013 (2013) 1-7.

[12] H. Moriyasu, K. Koshi, A. Sato, T. Suzuki, A. Nakagaito, M. Kouzu, Preparation of CaO catalyst from calcined limestone by mechanical grinding for biodiesel production, J. of Japan Institute of Energy 91 (2012) 495-502.

[13] M. L. Granados, A. C. Alba-Rubio, F. Vila, D. Martin Alonso, R. Mariscal, Surface chemical promotion of Ca oxide catalyst in biodiesel production reaction by the addition of monoglycerides, diglycerides and glycerol. Journal of Catalysis; 276 (2010) 2 229-236.

[14] Y. Xi, R. J. Davis, Influence of water on the activity and stability of activated Mg-Al hydrotalcites for the transesterification of tributyrin with methanol, J. Catal. 254 (2008) 190-197.

[15] M. Kouzu, M. Tsunomori, S. Yamanaka, J. Hidaka, Solid base catalysis of calcium oxide for a reaction to convert vegetable oil into biodiesel, Adv. Powder Technol. 21 (2010) 488-494.

[16] A. A. Refaat, Biodiesel production using metal oxide catalysts, Int. J. of Environ. Sci & Technol. 8 (2011) 203-221.

[17] I. Lukic, Z. Kesic, M. Zdujic, D. Skala, Calcium diglyceroxide synthesized by

mechanochemical treatment, its characterization and application as catalyst for fatty acid methyl esters production, Fuel 165 (2016) 159-165.

[18] M. Kouzu, T. Kasuno, M. Tajika, S. Yamanaka, J. Hidaka, Active phase of calcium oxide used as solid base catalyst for transesterification of soybean oil with refluxing methanol, Applied Catalysis A: General 334 (2008) 357-365.

[19] S. Yamanaka, A. Suzuma, T. Fujimoto, Y. Kuga, production of scallop shell nanoparticles by mechanical grinding as a formaldehyde adsorbent, J. Nanopart. Res. 15 (2013) 1573-1581.

[20] M. Hasegawa, M. Kimata, M. Shimane, T. Shoji, M. Tsurata, The effect of liquid additives on dry ultrafine grinding of quartz, Powder Technology 114 (2001) 145-151.

[21] A. M. Kalinkin, E. V. Kalinkina, O. A. Zalkind, T. I. Makarova, Chemical interaction of calcium oxide and calcium hydroxide with $CO_2$ during mechanical activation, Inorganic Material 41 (10) (2005) 1073-1079.

[22] P. L. Guzzo, J. B. Santos, R. C. David, Particle size distribution and structural change in limestone ground in planetary ball mill, Int. J. of Mineral Proc. 126 (2014) 41-48.

[23] Z. Kesic, I. Lukic, D. Brkic, M. Zdujic, H. Liu, et al., Mechanochemical preparation and characterization of CaO.ZnO used as catalyst for biodiesel synthesis, Appl Catal Gen 427-428 (2012)58-65.

[24] A. Kawashima, K. Matsubara, K. Honda, Development of heterogeneous base catalysts for biodiesel production, Bioresour. Technol. 99 (2008) 3439-3443.

[25] N. Kaur, A. Ali, Kinetics and reusability of Zr/CaO as heterogeneous catalyst for the ethanolysis and methanolysis of Jatropha crucas oil, Fuel Processing Technology 119 (2014) 173-184.

[26] A. Kawashima, K. Matsubara, K. Honda, Acceleration of catalytic activity of calcium oxide for biodiesel production, Bioresour. Technol. 100 (2009) 696-700.

[27] C. Plank, E. Lorbeer, Simultaneous determination of glycerol, and mono-, di- and triglycerides in vegetable oil methyl esters by capillary gas chromatography, J. of Chromatography A 697 (1995) 461-468.

[28] T. Watanabe, J. Liao, M. Senna, Changes in the basicity and species on the surface of $Me(OH)_2$-$SiO_2$ (Me = Ca, Mg, Sr) mixtures due to mechanical activation, J. of Solid State Chemistry 115 (1995) 390-394.

[29] M. S. Kaliszewski, A. H. Heuer, Alcohol interaction with zirconia powders, J. Am. Ceram. Soc. 73 (6) (1990) 1504-1509.

[30] M. Senna, Chemical powder technology – a new insight into atomic processes on the surface of fine particles, Advanced Powder Technol. 13 (2) (2002)

115-138.

[31] M. L. Granados, M. D. Zafra Poves, D. Martin Alonso, R. Mariscal, F. Cabello Galisteo, et al, Biodiesel from sunflower oil by using activated calcium oxide, Applied Catalysis B: Environmental 73 (2007) 317-326.

[32] J. Kondo, Y. Sakata, K. Maruya, K. Tamaru, T. Onishi, Infrared studies of methanol adsorbed on magnesium oxide, Applied Surface Science 28 (1987) 475-478.

[33] C. T. Vo, L. K. Huynh, J. –Y. Hung, J. Chaing Jiang, Methanol adsorption and decomposition on ZnO (1010) surface: a density functional theory study, Applied Surface Science 280 (2013) 219-224.

[34] H. Jeziorowski, H. Knozinger, W. Meye, H. D. Muller, H-bonding on solid oxide surfaces. Infra-red spectroscopic study of the adsorption of alcohols on silica and alumina, J. Chem., Faraday Trans, 1, 69 (1973) 1744-1758.

[35] Y. Tang, L. Li, S. Wang, Q. Cheng, J. Zhang, Tricomponent coupling biodiesel production catalyzed by surface modified calcium oxide, Environmental Progress & Sustainable Energy 35 (1) (2016) 257-262.

[36] X. Liu, X. Piao, Y. Wang, S. Zhu, H. He, Calcium methoxide as a solid base catalyst for the transesterification of soybean oil to biodiesel with methanol, Fuel 87 (2008) 1076-1082.

[37] M. Weibel, R. K. Mishra, Comprehensive understanding of grinding aids, ZKG 6 (2014) 29-39.

[38] X. Liu, X. Piao, Y. Wang, S. Zhu, Model study of transesterification of soybean oil to biodiesel with methanol using solid base catalyst, J. Phys. Chem. A. 114 (2010) 3750-3755.

[39] R. Song, D. Tong, J. Tang, C. Hu, Effect of composition on the structure and catalytic properties of KF/Mg-La solid base catalysts for biodiesel synthesis via transesterification of cottonseed oil, Energy Fuels 25 (2011) 2679-2686.

[40] M. Sanchez-Chantu, L. M. Perez-Diaz, I. Pala-Rosas, E. Cadena-Torres, L. Juarez-Amador, et al., Hydrated lime as an effective heterogeneous catalyst for transesterification of castor oil and methanol, Fuel 110 (2013) 54-62.

[41] H. Petitjean, H. Guesmi, H. Lauron-Pernot, G. Costentin, D. Loffreda, et al., How surface hydroxyls enhance MgO reactivity in basic catalysis: the case of methylbutynol conversion, ACS Catal. 4 (2014) 4004-4014.

[42] M. Kouzu, J. Hidaka, K. Wakabayashi, M. Tsunomori, Solid base catalysis glyceroxide for a reaction to convert vegetable oil into its methyl esters. Applied Catalysis A: General 390 (2010) 11-18.

## Supplementary material captions

## Experimental details

**Fig. S1:** (a) XRD patterns, and (b) FTIR spectra of scallop shells thermally calcined at 1000 °C for 3 h.

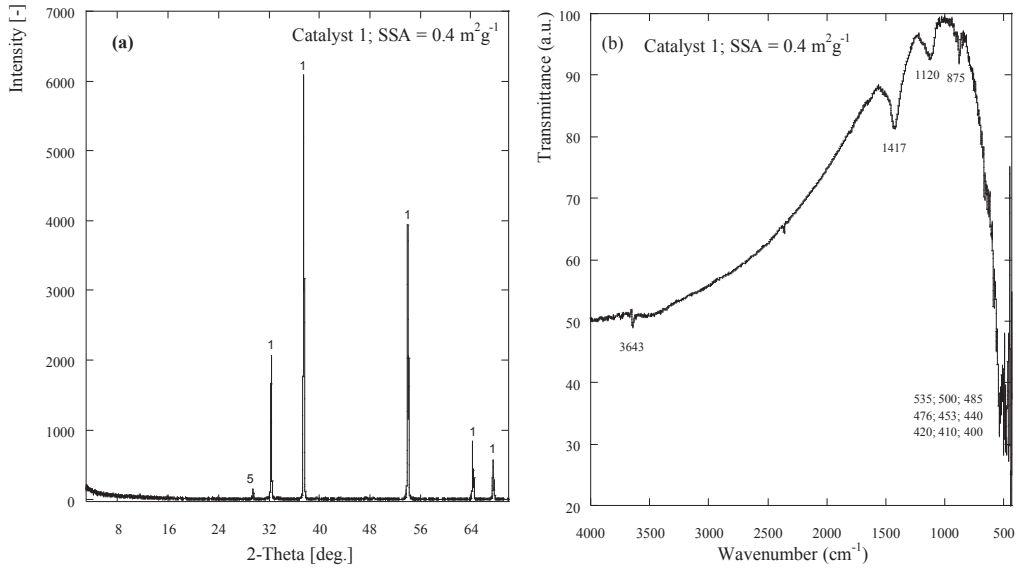


**Fig. S2:** FTIR spectra for scallop shells after processing by methanol-assisted dry nano-grinding. The nano-grinding conditions are listed in **Table 1**.

(5) $CaCO_3$, ICDD file 47-1743

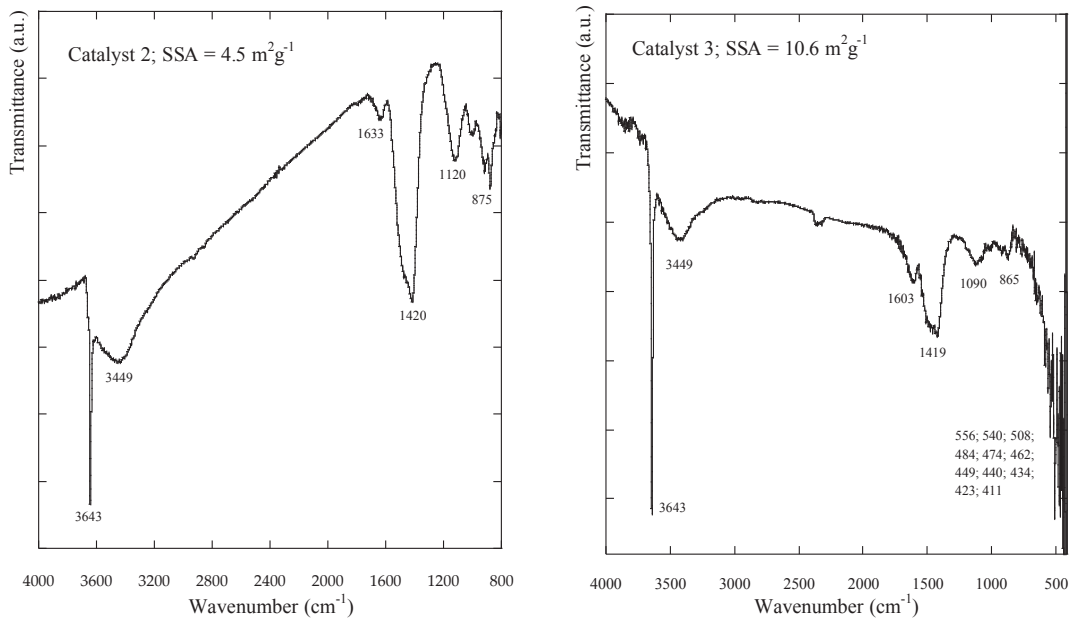

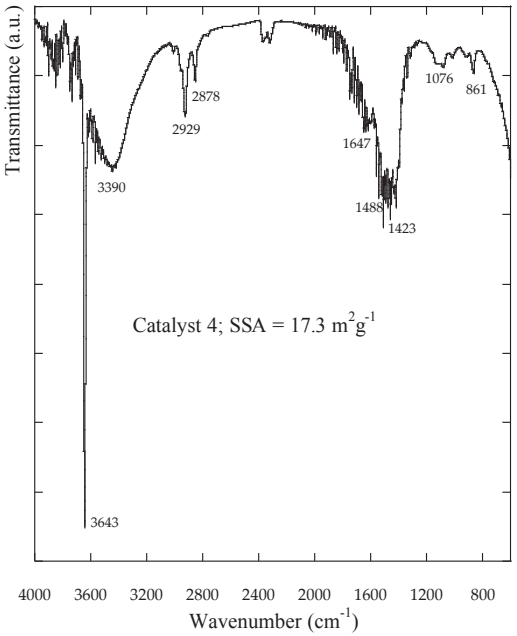
Transmittance (a.u.)
Catalyst 4; SSA = 17.3 m2g-1
3643
3390
2929
2878
1647
1488
1423
1076
861
4000 3600 3200 2800 2400 2000 1600 1200 800
Wavenumber (cm-1)

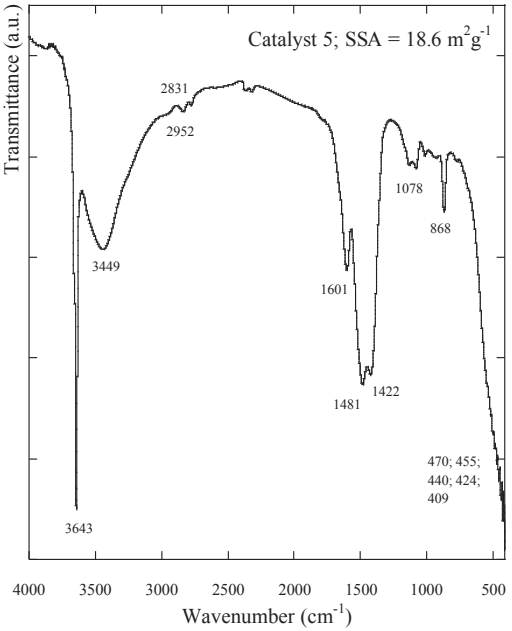
Transmittance (a.u.)
Catalyst 5; SSA = 18.6 m2g-1
3643
3449
2952
2831
1601
1481
1422
1078
868
470; 455;
440; 424;
409
4000 3500 3000 2500 2000 1500 1000 500
Wavenumber (cm-1)

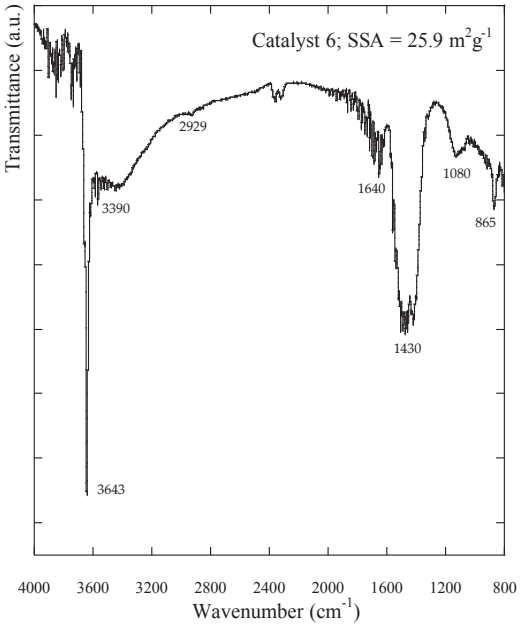
Transmittance (a.u.)
Catalyst 6; SSA = 25.9 m2g-1
3643
3390
2929
1640
1430
1080
865
4000 3600 3200 2800 2400 2000 1600 1200 800
Wavenumber (cm-1)

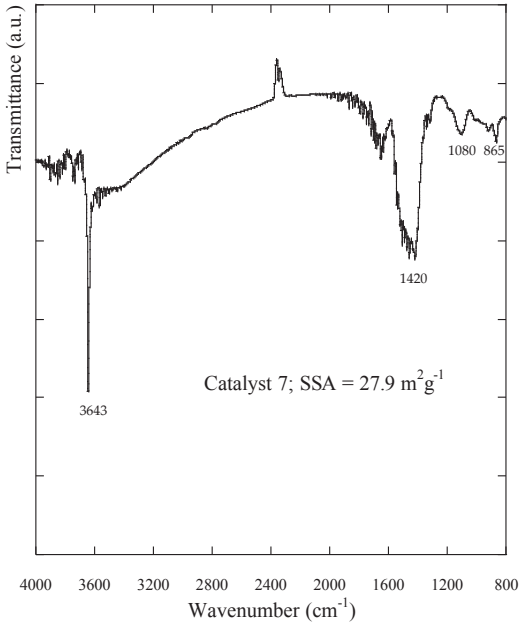
Transmittance (a.u.)
Catalyst 7; SSA = 27.9 m2g-1
3643
1420
1080 865
4000 3600 3200 2800 2400 2000 1600 1200 800
Wavenumber (cm-1)

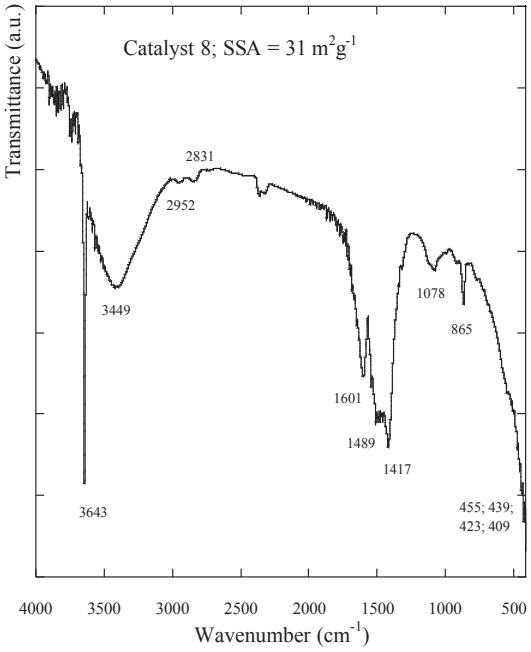
Catalyst 8; SSA = 31 m²g⁻¹
Transmittance (a.u.)
2831
2952
3449
1078
865
1601
1489
1417
3643
455; 439;
423; 409
4000 3500 3000 2500 2000 1500 1000 500
Wavenumber (cm⁻¹)

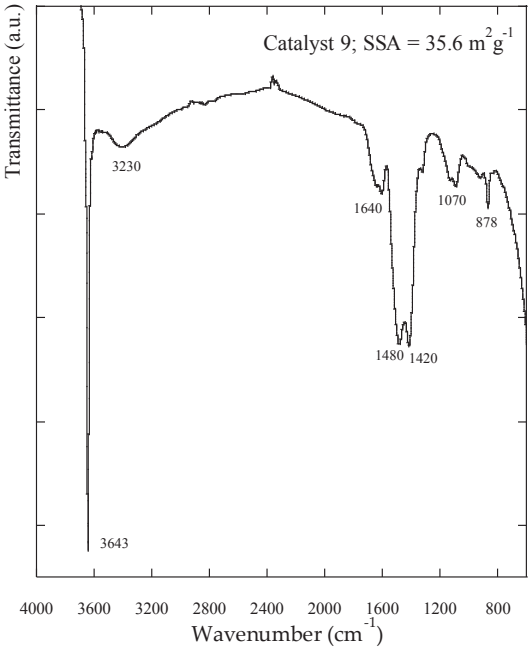
Catalyst 9; SSA = 35.6 m²g⁻¹
Transmittance (a.u.)
3230
1640
1070
878
1480
1420
3643
4000 3600 3200 2800 2400 2000 1600 1200 800
Wavenumber (cm⁻¹)

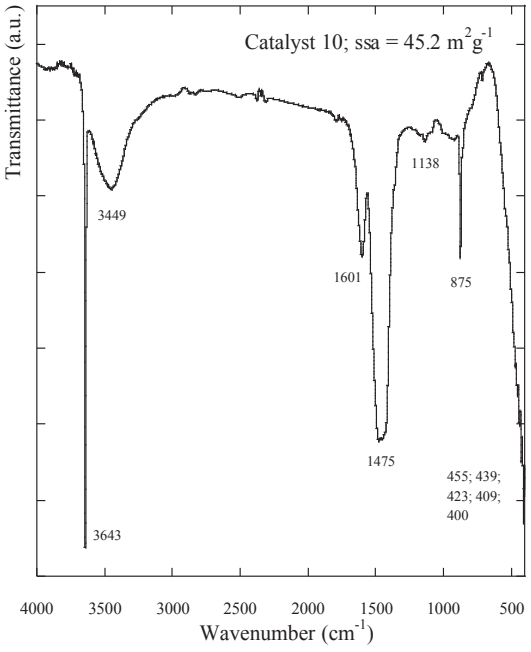
Catalyst 10; ssa = 45.2 m²g⁻¹
Transmittance (a.u.)
1138
3449
1601
875
1475
455; 439;
423; 409;
400
3643
4000 3500 3000 2500 2000 1500 1000 500
Wavenumber (cm⁻¹)

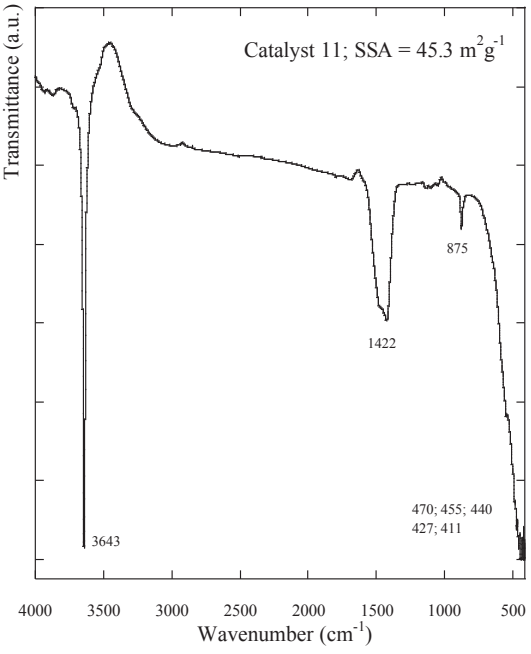
Catalyst 11; SSA = 45.3 m²g⁻¹
Transmittance (a.u.)
875
1422
470; 455; 440
427; 411
3643
4000 3500 3000 2500 2000 1500 1000 500
Wavenumber (cm⁻¹)

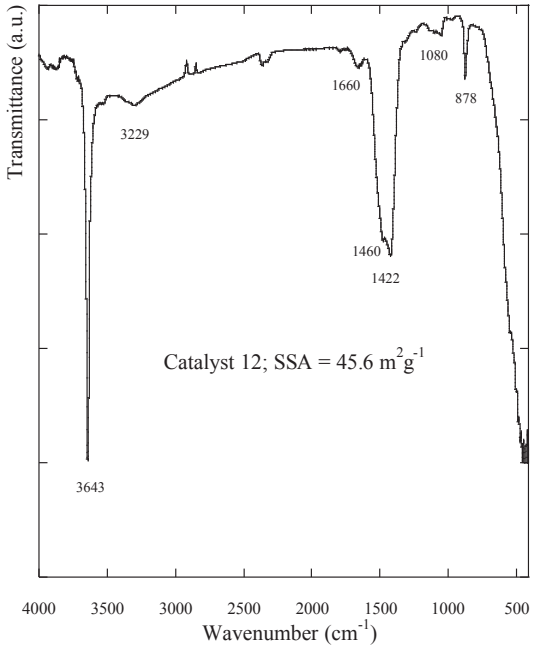
Transmittance (a.u.)
3643
3229
1660
1460
1422
1080
878
Catalyst 12; SSA = 45.6 m2g-1
4000 3500 3000 2500 2000 1500 1000 500
Wavenumber (cm-1)

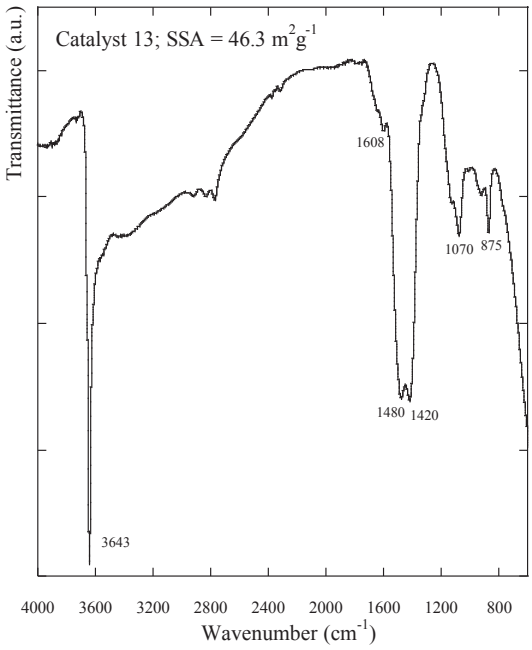
Transmittance (a.u.)
Catalyst 13; SSA = 46.3 m2g-1
3643
1608
1480
1420
1070
875
4000 3600 3200 2800 2400 2000 1600 1200 800
Wavenumber (cm-1)

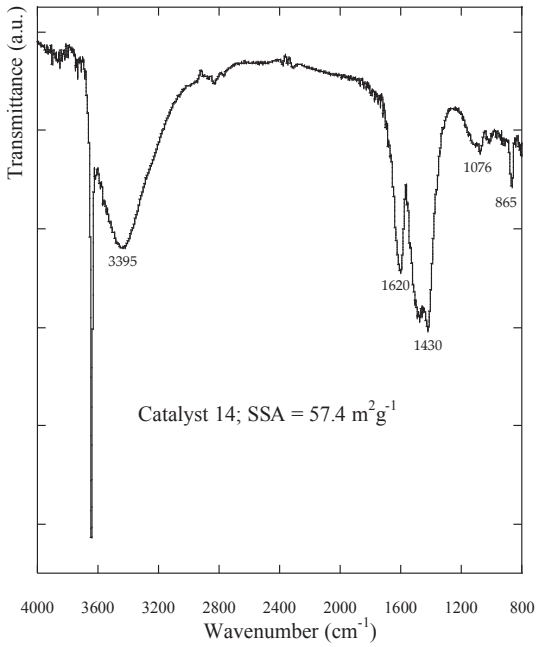
Transmittance (a.u.)
3395
1620
1430
1076
865
Catalyst 14; SSA = 57.4 m2g-1
4000 3600 3200 2800 2400 2000 1600 1200 800
Wavenumber (cm-1)

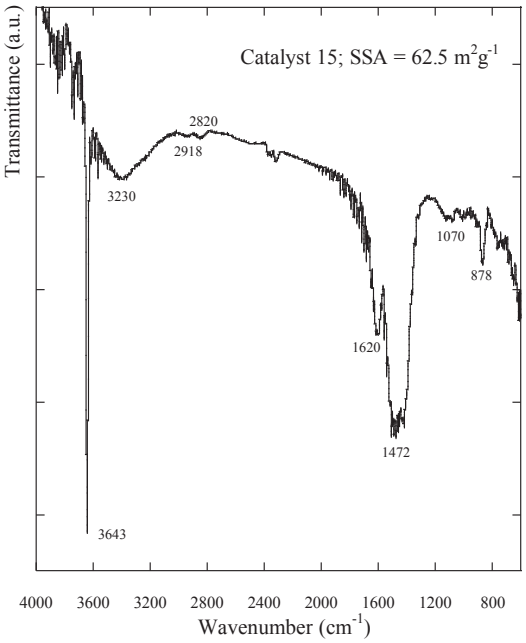
Transmittance (a.u.)
Catalyst 15; SSA = 62.5 m2g-1
3643
3230
2820
2918
1620
1472
1070
878
4000 3600 3200 2800 2400 2000 1600 1200 800
Wavenumber (cm-1)